Anomalous transport in cellular flows: The role of initial conditions and aging

Patrick Pöschke* and Igor M. Sokolov
Institute of Physics, Humboldt University of Berlin, D-12489 Berlin, Germany

Alexander A. Nepomnyashchy
Department of Mathematics, Technion—Israel Institute of Technology, Haifa 32000, Israel

Michael A. Zaks
Institute of Physics and Astronomy, University of Potsdam, D-14469 Potsdam, Germany
(Received 12 July 2016; published 23 September 2016)

We consider the diffusion-advection problem in two simple cellular flow models (often invoked as examples of subdiffusive tracer motion) and concentrate on the intermediate time range, in which the tracer motion indeed may show subdiffusion. We perform extensive numerical simulations of the systems under different initial conditions and show that the pure intermediate-time subdiffusion regime is only evident when the particles start at the border between different cells, i.e., at the separatrix, and is less pronounced or absent for other initial conditions. The motion moreover shows quite peculiar aging properties, which are also mirrored in the behavior of the time-averaged mean squared displacement for single trajectories. This kind of behavior is due to the complex motion of tracers trapped inside the cell and is absent in classical models based on continuous-time random walks with no dynamics in the trapped state.

DOI: 10.1103/PhysRevE.94.032128

I. INTRODUCTION

Anomalous diffusion in cellular flows has drawn considerable attention as a model showing a nontrivial intermediate asymptotic regime corresponding to subdiffusion and is reviewed, e.g., in [1] and [2]. A simple explanation (e.g., given in [2]) places this model in a class of close relatives of the comb models. In a comb, diffusion on a spine (say, in the x direction) is interrupted by the diffusion in the teeth (dangling ends) extending in the y direction and can be described by the continuous-time random walk (CTRW) in the x direction, with the waiting times distributed according to a power law. This diffusion is anomalous (subdiffusion) and, like diffusion in other CTRW models with power-law waiting times, shows aging and weak ergodicity breaking (see, e.g., [3]). Moreover, the properties of such diffusion strongly depend on the initial conditions.

The similarity between the cellular flow and the comb structures arises from the fact that, being trapped inside a single eddy cell, the particles cannot take part in the macroscopic diffusion unless returning to the separatrix between the cells, so that the coarse-grained picture of the macroscopic motion is again the CTRW. In this respect, diffusion in a cellular flow corresponds to the comb model with finite teeth, since the power-law waiting time at a site (inside the cell) has an exponential cutoff implied by the finite size of the trapping domain. Under such conditions the final asymptotic behavior of transport should be diffusive, with the effective diffusion coefficient $D^* \propto D\mathrm{Pe}^{1/2}$, where D is the coefficient of molecular diffusion, and Pe is the Péclet number, [4–8]. The employed mathematical approaches are based on homogenization (see, e.g., [9] and references therein) and on the large deviation theory [10]. Analytical predictions are compared to numerical simulations of the transport in the corresponding time range.

Remarkably, the prominent subdiffusive intermediate asymptotics remains much less investigated. The diffusion in cellular flows in this regime is sometimes considered as an example of a situation where aging and ergodicity breaking take place (see, e.g., [11] and [12]), without paying much attention to the peculiarity of this problem caused by the complicated dynamics inside the trapped state. The transport in cellular flows has been measured experimentally [13,14] (see also [15] and [16]). We are not aware of extensive numerical simulations of the stochastic differential equations for these systems or comparison of the numerics with the theoretical predictions in Ref. [4] and subsequent works even for the simplest initial conditions, corresponding to starting on the cell boundary (separatrix), or of any work considering aging and convergence to ergodic behavior in this context. Our work aims at filling this gap. In what follows two standard variants of cellular flows are considered: the eddy lattice (EL) flow in two dimensions (see, e.g., [8]), with the stream function given by

$$\psi_{\mathrm{EL}}(x,y) = ua \sin\left(\frac{x}{a}\right) \sin\left(\frac{y}{a}\right); \tag{1}$$

and a flow corresponding to a one-dimensional arrangement of cells along the x axis, with no-slip boundary conditions at $y = 0$ and $y = \pi a$. The model stream function is

$$\psi_{\mathrm{YPP}}(x,y) = ua \sin\left(\frac{x}{a}\right)\left(\frac{y}{\pi a}\right)^2\left(1 - \frac{y}{\pi a}\right)^2. \tag{2}$$

Introduced in [4], this flow is referred to below as the Young-Pumir-Pomeau (YPP) flow. In both cases u is the characteristic velocity, and πa is the cell size. Both flows show the intermediate-time subdiffusive behavior crossing over to normal diffusion at longer times. The comparison of these two flows is of considerable interest, since the transport behavior

*poeschke@physik.hu-berlin.de

in them is very similar in certain respects, but very different in others.

Below, in Sec. II we review the subdiffusion dynamics from the point of view of characteristic time scales. The problem is formulated and numerical procedures for direct simulation of stochastic differential equations are introduced in Sec. III. Results, concerning different aspects of transport, are presented in Sec. IV. Finally, in Sec. V we summarize our findings.

II. CHARACTERISTIC TIMES

Let us first briefly discuss the type of subdiffusive behavior and the characteristic times at which it can be observed. This discussion is a slight modification of the one in Ref. [4], so that no more detail than necessary is given here. The corresponding results are not new but will be of importance in what follows.

The trapping of the particle inside the flow cell is due to its diffusion in the direction transverse to the streamlines since, having entered the cell, the particle cannot leave it unless returning to its periphery. The particle motion in the direction normal to the streamlines (denoted below the z direction, with $z = 0$ corresponding to the separatrix) is obtained by averaging the diffusion-advection equation along the streamlines [4]. The averaged equation has the form of the diffusion equation,

$$\frac{\partial}{\partial t}p(z,t) = \frac{\partial}{\partial z}\left[D(z)\frac{\partial}{\partial z}p(z,t)\right]. \tag{3}$$

The z dependence of the diffusion coefficient is sensitive to the boundary conditions at the cell edges and therefore depends on the type of flow. For the free boundaries of the EL flow $D(z)$ can be taken constant and equal to the coefficient of the molecular diffusion; for the no-slip boundary conditions on the horizontal sides of the cell of the YPP flow one has to assume $D(z) \simeq z^{-1}$ for $z \ll a$ (see [4]).

The (intermediate) asymptotic behavior of the waiting-time probability density function (WTD) for the jumps from separatrix to separatrix can be obtained by first solving Eq. (3) for the probability of being at the origin $p(0,t)$ and then connecting this with the first return probability via the renewal approach, assuming the Markovian character of the process, by solving the integral equation $p(0,t) = \delta(0)\delta(t) + \int_0^t \phi(t')p(0,t-t')dt'$, which can be easily done in the Laplace domain. The power-law decay of $p(0,t) \propto t^{-\gamma}$ then translates into the behavior

$$\phi(t) \propto t^{\gamma-2} \tag{4}$$

for the first return-time probability density. Note that this discussion corresponds to the case where the particle starts on the separatrix ($z = 0$) and is pertinent to all transitions between the cells. The first waiting time will differ in all cases when the particle does not start at the separatrix, i.e., for different initial conditions (e.g., starting at the center) or in aged situations [17].

The behavior of $p(0,t)$ is

$$p(0,t) \propto \begin{cases} t^{-1/2} & \text{for EL flow,} \\ t^{-1/3} & \text{for YPP flow,} \end{cases} \tag{5}$$

which translates into $\phi(t) \propto t^{-3/2}$ (normal Sparre-Andersen behavior) for EL flow and into $\phi(t) \propto t^{-5/3}$ for YPP flow, respectively. Considering the corresponding CTRW between cells with step size a yields subdiffusion with

$$\langle R^2(t)\rangle \propto t^{1-\gamma} = \begin{cases} t^{1/2} & \text{for EL flow,} \\ t^{2/3} & \text{for YPP flow} \end{cases} \tag{6}$$

(see [18] and references therein). The power-law behavior as given by Eq. (4) takes place in a finite time range bounded from below and from above by two characteristic times, t_1 and t_2. The longer characteristic time, t_2, corresponds to the time of free molecular diffusion over the cell length, $t_2 \sim a^2/D$, and for $t > t_2$ the WTD $\phi(t)$ shows an exponential cutoff [4]. This time marks the crossover from the anomalous regime to normal diffusion.

The shorter characteristic time, t_1, does not follow from the preaveraged Eq. (3) and is the minimal time necessary to traverse the cell. It is different for the cases of free and no-slip boundary conditions. Note that this minimal time defines the normalization constant of the WTD $\phi(t)$. Since $\phi(t)$ vanishes rapidly both for $t \ll t_1$ and for $t \gg t_2$ one has

$$\int_{t_1}^{t_2} \phi(t)dt \simeq 1, \tag{7}$$

where, due to the fact that $\phi(t) \simeq t^{\gamma-2}$ is integrable, the upper bound is irrelevant, provided $t_2 \gg t_1$. Therefore

$$\phi(t) \simeq t_1^{1-\gamma} t^{\gamma-2}. \tag{8}$$

The shorter cutoff time thus defines the coefficient of the anomalous diffusion in the anomalous regime

$$\langle R^2(t)\rangle \simeq \frac{a^2}{t_1^{1-\gamma}} t^{1-\gamma} \tag{9}$$

up to a numerical constant. For the free boundary the minimal travel time is defined by the characteristic velocity of the flow and is of the order of $t_1 = a/u$. For the no-slip condition this is no more the case since the velocity in the boundary region vanishes.

Let us consider particles in the YPP flow entering a cell on its left side. During the time $t \sim a/u$ of travel along the vertical border of the cell the particle can move diffusively in the horizontal direction at a distance $\delta \sim \sqrt{Dt} \simeq (Da/u)^{1/2} \propto a\mathrm{Pe}^{-1/2}$, with $\mathrm{Pe} = ua/D$ being the Péclet number of the flow. This is the thickness of the boundary layer, as discussed in Appendix C of [4]. The streamline at this distance from the vertical boundary is characterized by the value of its stream function $\psi \simeq Au\delta$, with A being a number constant. When moving parallel to the horizontal boundary (say, for $x = 1/2$, where $\phi = By^2$) a tracer passes at the distance $y \propto \sqrt{a\delta}$ from it. The typical velocity at this horizontal part of the streamline is $v_x \simeq u(y/a) \sim u\sqrt{\delta/a}$. Therefore the typical transport time in the horizontal direction would be

$$t_1 \simeq \frac{a}{v_x} \propto \frac{a}{u}\mathrm{Pe}^{1/4}. \tag{10}$$

The ratio of the times t_2, which defines the end of the subdiffusion regime and the transition from anomalous diffusion to normal diffusion, and t_1,

$$\frac{t_2}{t_1} \propto \frac{a^2}{D}\frac{u}{a}\mathrm{Pe}^{-1/4} = \mathrm{Pe}^{3/4}, \tag{11}$$

is a growing function of the Péclet number, so that there is enough time for developing diffusion anomaly at high Péclet numbers in a YPP flow.

Summarizing these findings, we have

$$\frac{t_2}{t_1} \simeq \begin{cases} \mathrm{Pe} & \text{for EL flow} \\ \mathrm{Pe}^{3/4} & \text{for YPP flow.} \end{cases} \tag{12}$$

This means that the anomalous diffusion is only pronounced in the case of high Péclet numbers.

The existence of the upper cutoff guarantees the convergence of the mean waiting time t^* within the cell, given by

$$t^* = \int_{t_1}^{t_2} t\phi(t)dt \simeq t_1^{1-\gamma} t_2^{\gamma} \tag{13}$$

$$= t_2 \left(\frac{t_2}{t_1}\right)^{\gamma-1} = \frac{a^2}{D}\left(\frac{t_2}{t_1}\right)^{\gamma-1} \tag{14}$$

for $t_2 \gg t_1$ and for $0 < \gamma < 1$. The diffusion coefficient in the final regime of normal diffusion is then $D^* \simeq a^2/t^* = D(t_2/t_1)^{1-\gamma}$. Inserting the expression for t_2/t_1 and the values of γ we arrive at

$$D^* \simeq D\mathrm{Pe}^{1/2} \tag{15}$$

for both flows. This form of D^* guarantees the smooth crossover from the anomalous behavior as given by Eq. (9) to the diffusive behavior $\langle R^2(t)\rangle \sim D^* t$ at the crossover time t_2.

We note that for initial conditions different from starting on the separatrix, and for aged situations, the distribution of the first waiting time until the jump between the cells $\phi_1(t)$ differs from $\phi(t)$ and cannot, in general, be obtained within the approach based on the streamline averaging.

III. SIMULATION

The particle motion under the influence of the flow and of molecular diffusion is described by the Langevin equation

$$\dot{\mathbf{r}} = \mathrm{rot}\,(0,0,\psi(\mathbf{r})) + \sqrt{2D}\boldsymbol{\xi}. \tag{16}$$

Here $\mathbf{r}$ is the instantaneous two-dimensional particle position, and $\boldsymbol{\xi} = (\xi_x,\xi_y)$ is a vector of two independent Gaussian noises with zero mean, unit width, and $\langle \xi_x(t)\xi_x(t')\rangle = \langle \xi_y(t)\xi_y(t')\rangle = \delta(t'-t)$. Taking a as the unit length and $t_2 = a^2/D$ as the time unit, we can rewrite this equation as

$$\dot{\mathbf{r}} = \mathrm{Pe}\ \mathrm{rot}\,(0,0,\Psi(\mathbf{r})) + \sqrt{2}\boldsymbol{\xi}, \tag{17}$$

with

$$\Psi(x,y) = \begin{cases} \sin(x)\sin(y) & \text{for EL flow,} \\ \sin(x)\left(\frac{y}{\pi}\right)^2\left(1-\frac{y}{\pi}\right)^2 & \text{for YPP flow.} \end{cases} \tag{18}$$

Equation (17) has been numerically integrated using the Heun algorithm. This scheme, a variant of the second-order Runge-Kutta method, is known to be one of the best algorithms for the integration of stochastic differential equations with additive noise [19]. The results, the particle trajectories $\mathbf{r}(t)$, are used for further analysis. The time step of integration is chosen so that in the absence of noise the displacement in the direction normal to streamlines and the corresponding variation of Ψ stay negligible during the full simulation time $t_{\max} = 100$. For both systems taking a time step equal to $1/(1000\mathrm{Pe})$ turned out to be sufficient. A typical trajectory for the EL flow is shown in Fig. 1.

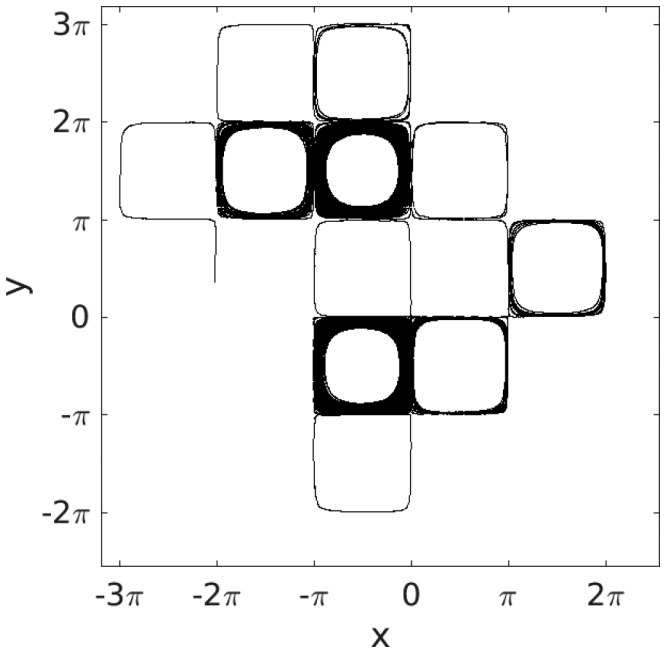

FIG. 1. A typical trajectory for the EL flow for $\mathrm{Pe} = 10^4$ starting at the origin.

The main quantities of interest are the mean squared displacement (MSD) of particles from their initial positions

$$\langle R^2(t)\rangle = \langle(\mathbf{r}(t) - \mathbf{r}(0))^2\rangle \tag{19}$$

for different initial conditions, the aged MSD (the MSD from the position a particle had at time t_a from the beginning of observation),

$$\langle R^2(t,t_a)\rangle = \langle(\mathbf{r}(t_a+t) - \mathbf{r}(t_a))^2\rangle, \tag{20}$$

and, respectively, the root mean squared displacement, which is the square root of the MSD, for $\Delta > 0$, the time-averaged MSD (TAMSD),

$$\overline{R^2(\Delta,T)} = \frac{1}{T-\Delta}\int_0^{T-\Delta} [\mathbf{r}(t'+\Delta) - \mathbf{r}(t')]^2\, dt', \tag{21}$$

and its ensemble-averaged analog,

$$\langle\overline{R^2(\Delta,T)}\rangle = \frac{1}{T-\Delta}\int_0^{T-\Delta} \langle[\mathbf{r}(t'+\Delta) - \mathbf{r}(t')]^2\rangle dt', \tag{22}$$

(for the essentially one-dimensional transport by YPP flow we only consider the displacements along the x axis), and the probability density function of the displacements from the initial position. The ensemble averaging corresponds to averaging over independent runs. If not stated otherwise, averaging over 10^4 independent tracers for $\mathrm{Pe} = 10^4$ was performed.

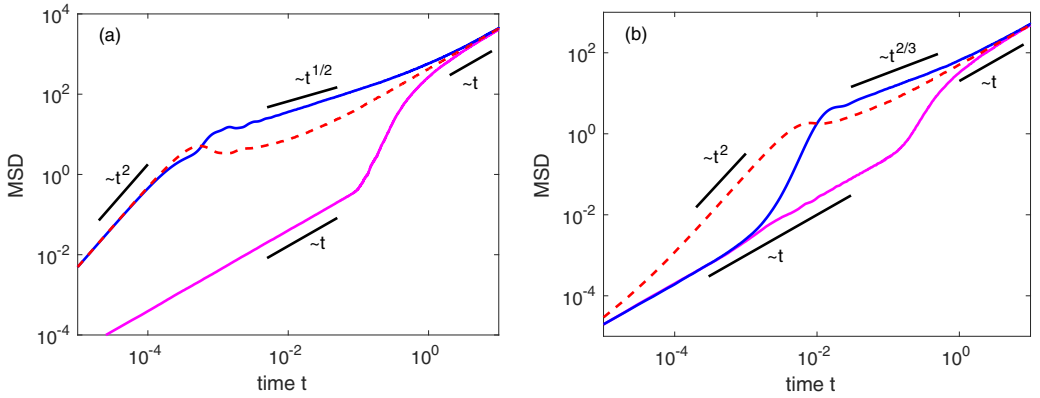

FIG. 2. MSD for Pe $= 10^4$ for (a) the EL flow and (b) the YPP flow starting at the separatrix (upper, solid blue line), in the flooded case (dashed red line), and starting at the center of a cell (lower, solid magenta line).

IV. RESULTS

The results for the main quantities of interest are shown in Figs. 2 to 4 and 6. In all these figures, (a) presents the results for the EL flow; (b), for the YPP flow.

Figure 2 shows the MSD for the corresponding flows for different initial conditions. The upper (solid blue) curves correspond to the situation where at the beginning the particles were homogeneously distributed on the separatrix, i.e., have $x(0) = 0$ and $y(0)$ homogeneously distributed between 0 and π. The lower curves (solid magenta) correspond to starting at the center of the cell, and the dashed red curves correspond to tracers initially homogeneously distributed within one cell. The latter situation is referred to as the "flooded case."

Let us first discuss the behavior of the MSD for a start at the boundary of the cell that, for $t > t_1$, is well described by CTRW. The curves exhibit three distinct regimes, for $t < t_1$, for $t_1 < t < t_2$, and for $t > t_2$. For the EL flow the motion for $t < t_1$ is dominated by the ballistic transport at the cell periphery. For the YPP flow the transport at short times (i.e., in the boundary layer) is dominated by the diffusion and not by the flow, so that the behavior for $t < t_1$ is diffusive. The transition from this domain to the next corresponds to a superballistic motion, since the transport velocity increases when the particle diffuses into the cell interior. The following regime of anomalous diffusion corresponds to $\langle R^2(t)\rangle \propto t^{1/2}$ for the EL flow and to $\langle R^2(t)\rangle \propto t^{2/3}$ for the YPP flow, as predicted by the CTRW model. The behavior for $t > t_2$ is diffusive for both flows.

The time evolution of the ensemble of tracers starting at the separatrix is indeed well described by the CTRW with the waiting-time densities $\phi(t) \propto \tau^\alpha t^{-1-\alpha}$ as given by Eq. (8), where the characteristic time τ is of the order of t_1 and $\alpha = 1 - \gamma$. Given $\phi(t)$ and the MSD per step a^2, the probability density function of the particle displacement in the Fourier-Laplace representation is

$$p(k,s) = \frac{\tau^\alpha s^{\alpha-1}}{k^2a^2/2 + \tau^\alpha s^\alpha} \tag{23}$$

for both k and s small, which corresponds to the long-time and large-scale limit in the space-time domain (see, e.g., Chap. 4 of Ref. [17]). The corresponding probability density function $p(x,t)$ in the space-time domain is an even function of its argument and scales as a function of $\rho = x/R(t)$, where $R(t) = \langle R^2(t)\rangle^{1/2}$ is the root mean squared displacement, $p(x,t) \propto f_\alpha[|x/R(t)|]$, with the scaling function $f_\alpha(\rho)$ depending on the index α as a parameter. For the YPP flow this can be found in quadratures [4],

$$f_{2/3}(\rho) \propto \mathrm{Ai}(\rho), \tag{24}$$

where $\mathrm{Ai}(\rho)$ is the Airy function (see Chap. 10 in [20]; also, note that $\rho > 0$). For the case of the EL flow ($\alpha = 1/2$) we are aware of no closed form, but a useful integral representation (see Chap. 6 in Ref. [17]) helps to find $p(x,t)$ [and thus $f_{1/2}(\rho)$] numerically,

$$p(x,t) \propto \int_0^\infty \frac{1}{\sqrt{K\omega t}} \exp\left(-\frac{x^2}{4K\omega} - \frac{\omega^2}{4t}\right) d\omega, \tag{25}$$

with K being proportional to the coefficient of the anomalous diffusion defining the MSD. Knowing $f_\alpha(\rho)$ we can build the corresponding cumulative distribution function (CDF) of the scaled absolute displacements ρ,

$$F_\alpha(\rho) = \frac{\int_0^\rho f_\alpha(z)dz}{\int_0^\infty f_\alpha(z)dz}, \tag{26}$$

and compare it to the numerical results, as shown in Fig. 3 (for the EL flow, only the displacement along the x direction is considered). The corresponding theoretical curves are shown as thick green lines. The results of the numerical evaluation of the corresponding CDFs of rescaled distances at different times are shown by thin lines. These do indeed roughly follow the CTRW predictions but show additional oscillations, which are not errors or artifacts but stem from the internal dynamics of particles within the cells, which is not resolved on the scales where the CTRW approach is applicable. It is exactly this intracell dynamics which makes the anomalous diffusion in cellular flow different from that in combs with finite teeth. Note also that the theoretical curves of CDF(ρ) for different, not too small Pe values should all coincide as well for both systems. We checked this to hold for 10 times larger Pe values, i.e., Pe $= 10^5$.

Let us return to our discussion of Fig. 2. When starting at the center of the cell (lower, solid magenta curves), no intermediate subdiffusion is seen, and the behavior in both EL and YPP flows corresponds to a superballistic crossover

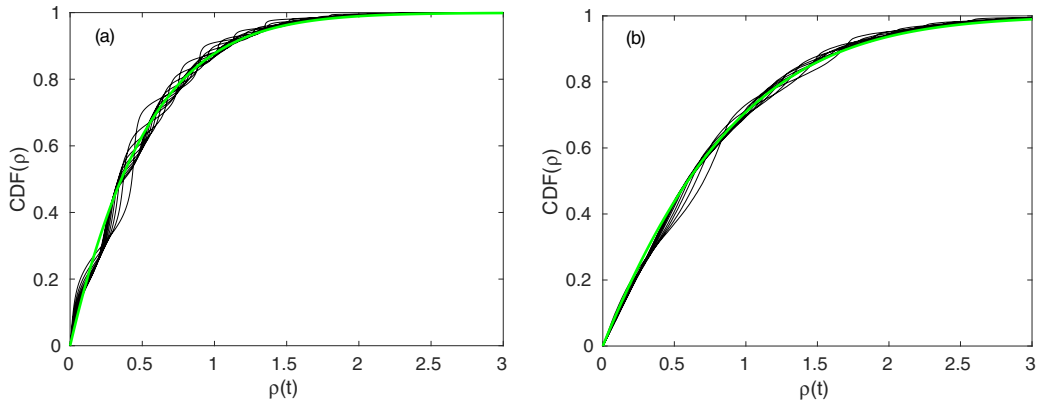

FIG. 3. (a) CDF for $\mathrm{Pe} = 10^4$ depending on the rescaled distance ρ for EL in the subdiffusive regime: 10^6 simulated walks with time $t \in [0.01,0.1]$ in steps of 0.01 (thin black line) compared to the predictions of the CTRW (thick green line). (b) The same for the YPP flow: 10^5 simulated walks of time $t \in [0.1,0.5]$ in steps of 0.05. Note that no adjustable parameters were used to obtain these two plots.

from short-time diffusion with diffusion coefficient D to final diffusion with $D^* \simeq D\mathrm{Pe}^{1/2}$.

When the initial positions of the particles are homogeneously distributed within the cell (dashed red curve), the long-time behavior is exactly like in the previous two cases. The short-time behavior is ballistic, which for the EL flow coincides with that obtained with a start at the separatrix. Note also that for the flooded case no intermediate domain with a constant diffusion exponent smaller than unity can be detected: The crossover from the initial ballistic to the final diffusive behavior involves only a slight oscillation. A similar behavior of the MSD for the considered initial conditions is seen also for smaller Péclet numbers (as low as 10^2) and for larger ones (up to 10^6, the upper limit for our simulations; not shown).

For the YPP flow we also take the fourth initial condition of particles starting at a wall, i.e., at $y = 0$ [see dotted black lines in Fig. 4(b)]. This initial condition is equivalent to starting at the separatrix with a vanishing advection flow and it corresponds to a pollution model of the atmosphere with dust being initially on Earth's surface. The aged MSD for this initial condition is very similar to the one for starting at the separatrix (solid blue curve). Only for short times, the MSD is approximately the one for starting at the center of a cell (magenta), because of the initially vanishing advection.

The strong dependence on the initial conditions is the reason for aging and for intermediate-time nonergodic behavior of the MSD (see, e.g., the discussion in [21]).

Let us first turn to the aging behavior of the MSD. Since the homogeneous distribution of particles within the system is invariant under diffusion and flow, the MSD for the initial condition, when the particles are distributed homogeneously within the cell, does not show any aging effects: $\langle R^2(t,t_a)\rangle = \langle R^2(t)\rangle$. For any other initial condition aging is present, as shown in Fig. 4, and the $\langle R^2(t)\rangle$ for the homogeneously flooded cell acts as the limiting curve for $\langle R^2(t,t_a)\rangle$ for $t_a \to \infty$. When starting at the separatrix, this limiting curve (in the intermediate-time domain corresponding to anomalous diffusion) is approached from above for both flows. In the short-time domain there is a difference between the EL and the YPP flows caused by different relative positions of the MSD curves discussed above. Since for the EL flow the short-time behavior for starting at the separatrix and for starting homogeneously within the cell coincide, the MSD at short times does not age. On the contrary, for the YPP flow it shows a distinct speedup. In the situation where the particle starts at the center of the cell, considerable aging effects are always observed. For EL the short-time behavior of the aged MSD is always ballistic and approaches the asymptotic (ballistic) short-time behavior from below. For the YPP flow the aged short-time MSD behavior shows the change of regime, from diffusive to ballistic.

The intermediate-time behavior of the aged MSD for $t_1 \ll t \ll t_2$ is the most interesting one. It is similar for both flows. As one readily infers from Fig. 4, the values of $\langle R^2(t,t_a)\rangle = \langle(\mathbf{r}(t_a+t) - \mathbf{r}(t_a))^2\rangle$ in the time domain above and for moderate $t_a \ll t_2$ are small compared to the squared cell size. Therefore this behavior is dominated by the complex dynamics within a single eddy and shows oscillations, whose amplitude decays slowly with an increase in both t and t_a. This kind of aging behavior is not observed in a comb model, which does not show any internal dynamics within the trapped state. The oscillations exhibited by the aged MSD are due to the fact that the tracer position after aging time t_a is not at the center but at a finite distance from it. The further motion of the tracer approximately follows a closed streamline around the center of the cell, and indeed the frequency of the oscillations corresponds to the angular velocity of such rotations, which (in our dimensionless units) follows from the solution of the deterministic part of Eq. (17) for $\mathbf{r}$ close to the center of the cell. These frequencies are $\omega = \mathrm{Pe}$ for the EL flow and $\omega = (4\pi)^{-1}\mathrm{Pe}$ for the YPP flow. Our simulations corroborate the findings for the corresponding time periods of the rotations for the examined Pe values. The decay of these oscillations is caused by the dephasing of the motion. In the course of time more and more particles move away from the center of the cell. On the other hand, the circulation frequency depends on the distance from the center and decays to 0 at its periphery.

For the EL flow an approximate formula for the oscillatory behavior of the MSD can be derived in the following way: Sufficiently close to the center of the cell the streamlines are nearly circular, and the diffusion occurs basically in the

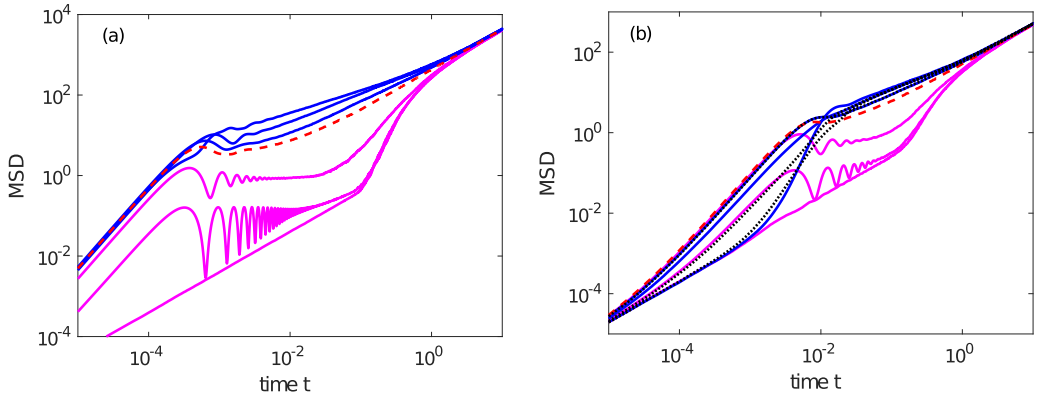

FIG. 4. Same as Fig. 2, with aging times $t_a = 0$, 10^{-2}, and 10^{-1} (upper, solid blue and lower, solid magenta curves) compared to the flooded case (dashed red curve). In (b) we show, in addition, the initial condition of starting at a wall, i.e., at $y = 0$ (dotted black curve).

radial direction, whereas angular distributions are practically uniform. Let the particles at time $t = -t_a$ be δ-distributed at the center of the cell. At $t = 0$ their probability density is then given by

$$p(r) = \frac{1}{4\pi D t_a} \exp\left(-\frac{r^2}{4Dt_a}\right), \tag{27}$$

with $D = 1$ in our units. Diffusion is assumed to be much slower than advection. Thus let us for the moment "freeze" the diffusion completely. We fix this distribution and assume that the tracers are uniformly advected along their respective circular streamlines. Then evolution of the MSD is governed by nonisochronicity of rotations. The larger the radius r, the longer the period $T(r)$. At time t, the instantaneous MSD for the infinitesimally thin ring of radius r equals

$$2r^2(1 - \cos(\omega(r)t)) \times 2\pi r p(r)\, dr, \tag{28}$$

with $\omega(r) = 2\pi/T(r)$. Thus the MSD equals $4\pi \int_0^\infty r^3 p(r)(1 - \cos(\omega(r)t))\, dr$. When shifting the origin of the coordinates to the center of a cell, i.e., with $x = \pi/2 + U/2$ and $y = \pi/2 + V/2$, the equations $\dot{\mathbf{r}} = \mathrm{Pe}\ \mathrm{rot}(0,0,\Psi(\mathbf{r}))$ become $\ddot{U} + \mathrm{Pe}^2 \sin(U) = 0$ and $\ddot{V} + \mathrm{Pe}^2 \sin(V) = 0$. Solutions of these pendulum equations are elliptic functions. For the oscillation of variable U with amplitude U_0, the period equals $T(r) = \frac{4}{\mathrm{Pe}} K(1 - \cos(U_0))$, with $K(m)$ being the complete elliptic integral of the first kind (see, e.g., Chap. 17 in [20]). For sufficiently low amplitudes the period obeys

$$T(r) = \frac{2\pi}{\mathrm{Pe}}\left(1 + \frac{1}{8}U_0^2 + \frac{19}{768}U_0^4 + \cdots\right), \tag{29}$$

with $U_0 = 2r$. Considering only terms up to quadratic order in r, we end up with $\omega(r) = \frac{2\pi}{T(r)} = \mathrm{Pe}(1 - \frac{r^2}{2})$. Substituting into the expression for the MSD and performing the integration yields

$$\langle R^2(t,t_a)\rangle = 8t_a + \frac{8t_a}{\left(1 + 4\mathrm{Pe}^2 t^2 t_a^2\right)^2}\left[\left(4\mathrm{Pe}^2 t^2 t_a^2 - 1\right)\cos(\mathrm{Pe}\, t) - 4\mathrm{Pe}\, t t_a \sin(\mathrm{Pe}\, t)\right]. \tag{30}$$

Now we "unfreeze" the diffusion stopped at t_a, i.e., we replace t_a with $t_a + t$. After the oscillations die out, the approximate expression becomes linear in time. Then the approximation does not hold any longer, since further terms in the expansion of the elliptic integral should be taken into account. Furthermore, the relevant streamlines of the EL flow are not circular anymore. However, for short times and short aging times, this approximation describes the MSD quite well, as we can see in Fig. 5, where the oscillating part of the aged MSD in Fig. 4(a) is compared to our obtained formula. A similar derivation for the YPP flow leads to much more elaborate expressions, since the streamlines are not circular even in the vicinity of the center.

The behavior of the time-averaged MSD, Eq. (21), strongly depends on the total averaging time. Here we report the results for $T \gg t_2 = 1$. For this case the ensemble-averaged TAMSD for particles starting at the separatrix displays the behavior changing from ballistic at short times to diffusive at long times, as shown in Fig. 6 (solid black lines), very similar to the behavior observed for initially homogeneously flooded cells. This intermediate stage disappears for low Pe, when t_1 and t_2 get too close. The overall type of the behavior can be explained by the discussion of a single trajectory, as shown in Fig. 1. Building a TAMSD with longer T corresponds to averaging

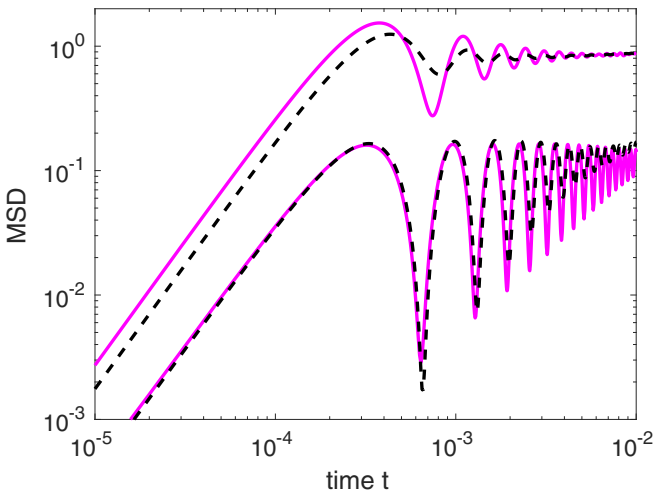

FIG. 5. Zoom-in on Fig. 4(a) compared to the approximate expression, Eq. (30) (dashed curve), with t_a replaced by $t_a + t$.

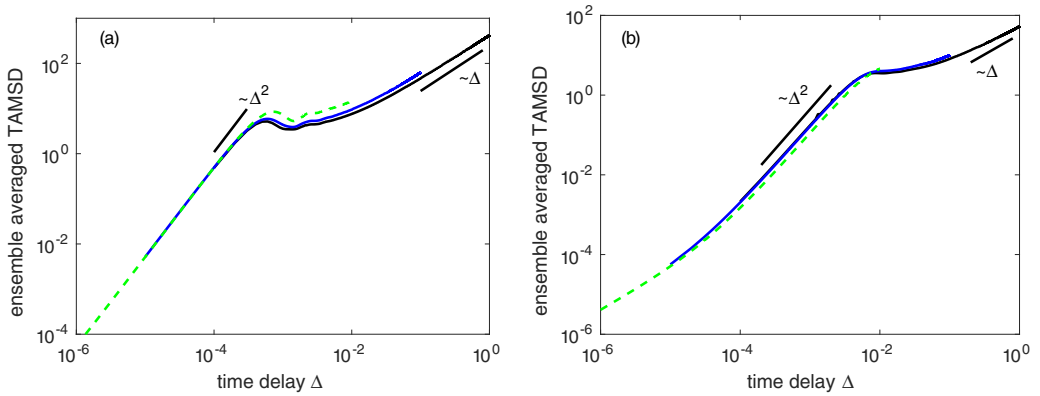

FIG. 6. $\langle\overline{R^2(\Delta,T)}\rangle$ for $\mathrm{Pe} = 10^4$ according to Eq. (22) starting at the separatrix averaged over 10^2 walks (a) for the EL flow and (b) for the YPP flow for $T = 10$ (solid black curve), $T = 1$ (solid blue curve), and $T = 0.1$ (dashed green curve).

over all possible positions which the particle assumes during its motion taken as the initial position. The distribution of these positions, reduced to a single cell, is relatively homogeneous. Since for $T \gg t_2$ the system homogenizes, the dependence on T, as well as the dependence on initial conditions, disappears, and the distribution of TAMSD around its ensemble average is relatively narrow. The situation here is similar to the case of the CTRW with the truncated power-law WTD as discussed in [11]. For T of about order unity (see the dashed green and solid blue curves in Fig. 6), the ensemble-averaged TAMSD is also already very similar to the MSD for the flooded case. For $T \ll t_2$ the typical ergodicity breaking behavior should be present, but the dependence on the initial conditions and the complicated internal dynamics within the trapped state make the situation much more involved than that for the pure CTRW (see [11] and [12]).

V. CONCLUSIONS

We have considered the diffusion-advection problem in two simple cellular flow models that differ with respect to the boundary conditions imposed on the cell edges. The models, often invoked as examples of subdiffusive tracer motion, were hardy investigated in detail. We concentrate on the intermediate time range, in which the tracer motion indeed may show subdiffusion. Extensive numerical simulations of the systems under different initial conditions show that the intermediate-time subdiffusion regime is only evident when the particles start at the border between different cells, i.e., at the separatrix, and is less pronounced or absent for other initial conditions, e.g., when particles initially are injected in the cell center or are homogeneously distributed within the cell. The complex motion of the particles within the single cell leads to peculiar aging properties of the system in this intermediate-time domain and is mirrored also in the behavior of the time-averaged mean squared displacement for single trajectories. Such behavior is not captured by classical models based on continuous-time random walks that possess no dynamics in the trapped state.

ACKNOWLEDGMENTS

We are thankful to Prof. Eli Barkai, whose questions provoked the present work. This work was financed by the German-Israeli Foundation for Scientific Research and Development (GIF) Grant No. I-1271-303.7/2014.

[1] J. P. Bouchaud and A. Georges, Phys. Rep. **195**, 127 (1990).
[2] M. B. Isichenko, Rev. Mod. Phys. **64**, 961 (1992).
[3] Y. Meroz, I. M. Sokolov, and J. Klafter, Phys. Rev. Lett. **107**, 260601 (2011).
[4] W. Young, A. Pumir, and Y. Pomeau, Phys. Fluids A **1**, 462 (1989).
[5] S. Childress, Phys. Earth Planet. Inter. **20**, 172 (1979).
[6] A. M. Soward, J. Fluid Mech. **180**, 267 (1987).
[7] B. I. Shraiman, Phys. Rev. A **36**, 261 (1987).
[8] M. N. Rosenbluth, H. L. Berk, I. Doxas, and W. Horton, Phys. Fluids **30**, 2636 (1987).
[9] A. J. Majda and P. R. Kramer, Phys. Rep. **314**, 237 (1999).
[10] P. H. Haynes and J. Vanneste, J. Fluid Mech. **745**, 321 (2014); **745**, 351 (2014).
[11] T. Miyaguchi and T. Akimoto, Phys. Rev. E **83**, 062101 (2011).
[12] T. Miyaguchi and T. Akimoto, Phys. Rev. E **87**, 032130 (2013).
[13] O. Cardoso and P. Tabeling, Europhys. Lett. **7**, 225 (1988).
[14] T. H. Solomon and J. P. Gollub, Phys. Fluids **31**, 1372 (1988).
[15] T. H. Solomon, E. R. Weeks, and H. L. Swinney, Phys. Rev. Lett. **71**, 3975 (1993).
[16] L. Bergougnoux, G. Bouchet, D. Lopez, and É. Guazzelli, Phys. Fluids **26**, 093302 (2014).
[17] J. Klafter and I. M. Sokolov, *First Steps in Random Walks* (Oxford University Press, Oxford, UK, 2011).
[18] G. Iyer and A. Novikov, Prob. Theory Relat. Fields **164**, 707 (2016).
[19] R. Mannella, in *Stochastic Processes in Physics, Chemistry, and Biology* (Springer, Berlin, 2000), p. 353.
[20] M. Abramowitz and I. A. Stegun, *Handbook of Mathematical Functions with Formulas, Graphs, and Mathematical Tables* (U.S. Government Printing Office, Washington, DC, 1964).
[21] I. M. Sokolov, Soft Matter **8**, 9043 (2012).